Remote Sensing Image Compression Based on Adaptive Directional Wavelet Transform With Content-Dependent Binary Tree Codec

Cuiping Shi, *Member, IEEE*, and Liguo Wang, *Member, IEEE*

***Abstract*—Remote sensing images provide a wealth of information for a variety of applications, but it is at the expense of huge data. In this paper, we present a novel compression method based on optimum adaptive directional lifting (OADL) with content-dependent binary tree codec. First, the OADL model is designed, which calculates the optimal prediction direction of each image block and performs the weighted directional adaptive interpolation during the process of lifting. The former aims to reduce the edge and texture energy of the non-horizontal and non-vertical directions in the high-frequency subbands, and the latter focuses on preserving the directional characteristics of remote sensing images as much as possible. Second, a binary tree codec with content-based adaptive scanning is introduced, which can provide different scanning orders and scanning manners among and within subbands, respectively. In addition, it can encode more significant coefficients at the same bit rate. Experimental results show that, compared with other scan-based compression methods, the proposed compression method can always provide better coding performance in terms of some evaluation indexes.**

***Index Terms*—Adaptive directional lifting (ADL), binary tree codec, compression, remote sensing images.**

I. Introduction

Along with the rapid development of sensor technology, the spatial resolution of remote sensing images increases dramatically, which is very beneficial to the applications of remote sensing images. However, abundant information means a huge amount of data, which also brings a great challenge to the storage and transmission of remote sensing images. Therefore, great efforts have been made in order to compress remote sensing images effectively. The research object of this paper is the panchromatic remote sensing image. Compared with the compression of traditional digital images, the compression of remote sensing images has a certain commonality, i.e., to remove the redundancy of images. On the other hand, the compression of remote sensing images has its particularity. Remote sensing images are acquired by a spaceborne or airborne imaging equipment with a large field of view (FOV), which usually contains a lot of ground objects. Therefore, most remote sensing images are of low space redundancy, and often contain some important details, such as contours of terrain, complex texture of objects, and even the outline of small targets. These details are very useful for some applications, such as geomorphic change detection, target anomaly detection, or classification, so they also should be preserved as far as possible during the process of the compression. Thus, the compression methods for traditional digital images that often ignore the high-frequency information while focusing on keeping the low-frequency information are not very applicable.

Generally, some traditional compression methods are widely used for the compression of images, such as embedded zerotree wavelet [1], set partitioning in hierarchical tree (SPIHT) [2], set partitioned embedded block coder (SPECK) [3], and Joint Photographic Experts Group 2000 (JPEG2000) [4], or some improvements on these algorithms [5]–[10]. In recent years, some compression methods that are specifically designed for remote sensing images have been proposed. The Consultative Committee for Space Data Systems (CCSDS) published a recommended standard of Image Data Compression (CCSDS-IDC) [11], [12], which specifically targets for onboard image compression. The CCSDS-IDC standard mainly focuses on the complexity of the algorithm but gives less attention to its flexibility. For example, the CCSDS fixes the level of wavelet decomposition to three and does not support interactive decoding. In [13], it makes some improvement on the CCSDS standards, which allows any level of wavelet decomposition and supports several ways of interactive decoding. Since remote sensing images are often acquired incrementally by sensors in a push-broom fashion, the scan-based compression methods are very desirable when handling remote sensing data [14]. In [15], it makes some improvements on JPEG2000 from the perspective of scanning way

Manuscript received February 22, 2018; revised November 30, 2018; accepted January 28, 2019. Date of publication March 14, 2019; date of current version March 25, 2019. This work was supported in part by the National Natural Science Foundation of China under Grants 41701479 and 61675051, in part by China Postdoctoral Science Foundation under Grant 2017M621246, in part by the Postdoctoral Science Foundation of Heilongjiang Province of China under Grant LBH-Z17052, in part by the Project Plan of Science Foundation of Heilongjiang Province of China under Grant QC2018045, in part by the Fundamental Research Funds in Heilongjiang Provincial Universities of China under Grant 135309342, and in part by the Science and Technology Plan Project of Qiqihar of China under Grant GYGG-201415. *(Corresponding author: Liguo Wang.)*

C. Shi is with the Department of Communication Engineering, Qiqihar University, Qiqihar 161000, China, and also with the College of Information and Communication Engineering, Harbin Engineering University, Harbin 150001, China (e-mail: scp1980@126.com).

L. Wang is with the College of Information and Communication Engineering, Harbin Engineering University, Harbin 150001, China (e-mail: wangliguo@hrbeu.edu.cn).

Color versions of one or more of the figures in this paper are available online at http://ieeexplore.ieee.org.

Digital Object Identifier 10.1109/JSTARS.2019.2897344

and provides a good compression performance for remote sensing images. However, the improvement of performance is at the expense of higher complexity. In order to realize the scan-based compression in a simple way, Huang and Dai [16] propose a binary tree coding adaptively (BTCA) method for the compression of remote sensing images, which scans the significant nodes and their brothers of a binary tree before scanning other nodes for each threshold, and can provide a good compression performance. Moreover, the complexity of it is very low. Although BTCA can protect some detailed information of images in the process of compression, which is somehow related to the characteristics of remote sensing images, it only takes the coding phase into consideration. Besides the compression methods mentioned above, some other compression algorithms are also applied for remote sensing images. In [17], the multi-spectral images are compressed by using an improved SPIHT. In [18], a compression method based on quadtree and zerotree coding for SAR complex images is proposed. In [19], it presents a hierarchical compression method for the progressive transmission of hyperspectral images. In [20], an onboard compression method based on quadtree coding is proposed, which is proved to be suitable for spaceborne equipment. Huang *et al.* [21] provide a coding method based on binary tree and optimize truncation, which improves the coding performance and is of the property of random access. However, these compression approaches are still designed only from the coding phase. For remote sensing images, due to their own characteristics, the ways of image representation will also have a great influence on the compression performance.

A lot of research has been done on image representation. In [22], an adaptive directional lifting (ADL)-based wavelet transform is proposed, which incorporates the spatial directional prediction into the conventional 2-D lifting structure. For the ADL-based method, a rate-distortion-optimized image segmentation is employed, which makes the ADL efficiently approximate image direction in local regions. The performance improvement is based on the ADL method, mainly due to the efficient image representation and coding of side information. However, for the image that is rich in details, the side information is often a heavy burden. Moreover, the interpolation of the ADL method favors only the horizontal and vertical directions, which may blur the orientation property and increase prediction error of images. These all prevent the ADL method from further improving the coding performance. Other image representation methods, such as [23]–[28], are often carried out from the perspective of the directional lifting wavelet, hybrid wavelets and directional filter banks, or tucker decomposition. After the image representation, an existing coding standard, such as SPIHT or JPEG2000, is usually followed directly. However, image representation and coding are different stages of compression, and the two stages are related. If only one stage is considered, the improvement of compression performance would be limited.

In this paper, in order to provide a good compression method for remote sensing images, both the process of image representation and coding are considered. First, we develop an optimum adaptive directional lifting (OADL) model for an effective representation of remote sensing images. Then, after the OADL-based wavelet transform, a binary tree codec with content-based adaptive scanning (BTCCA) is introduced, which can provide good coding performance with low complexity.

Our main contributions in this paper are listed as follows.

1) A new OADL model is designed considering the characteristics of remote sensing images. It can preserve more directional information of remote sensing images by utilizing the optimal direction prediction and the weighted directional adaptive interpolation. Moreover, there is no need to store the image-dependent adaptive segmentation tree as the side information.
2) A simple and efficient coding method is presented. After the proposed lifting-based wavelet transform, the energy of remote sensing images is more concentrated, which usually "enlarges" the difference among subbands due to the content of images. This coding method can provide different scanning orders and scanning methods among and within subbands and can encode more significant coefficients at the same bit rate.

The remainder of this paper is organized as follows: In Section II, the proposed OADL-based wavelet transform method is described in detail. In Section III, we analyze the content-based adaptive scanning method first, and then the BTCCA method is introduced. Section IV gives some quality evaluation index used in this paper. In Section V, some numerical experiments are performed, and the high effectiveness of the proposed compression method is proved. Finally, the conclusions are provided in Section VI.

II. Wavelet Transform With OADL

The traditional two-dimensional (2-D) lifting wavelet transform only uses the neighboring elements in the horizontal or vertical direction. However, for the texture or edge of an image is neither horizontal nor vertical, the traditional lifting scheme fails to provide effective representation for that directional information. Therefore, the idea of directional prediction is incorporated into the traditional 2-D lifting structure, which predicts an element by the direction with smaller prediction error. The existing directional wavelet transforms tends to be designed without considering the characteristics of remote sensing images. In this paper, an OADL-based wavelet transform is proposed, which is specifically designed for remote sensing images and can provide a good representation for it.

A. Structure of Adaptive Directional Lifting Scheme

Without loss of generality, suppose an image is first decomposed into a low-frequency subband and a high-frequency subband by a 1-D wavelet transform in the horizontal direction. Following, the same operation is performed by a 1-D wavelet transform in the vertical direction. The typical lifting process consists of four stages: split, predict, update, and normalize [29], [30]. The 1-D directional lifting wavelet transform and inverse transform are shown in Fig. 1(a) and (b), respectively.

Considering a 2-D image $x(m, n)_{m,n \in Z}$. First, all samples of the image are split into two parts: the even sample subset x_e and

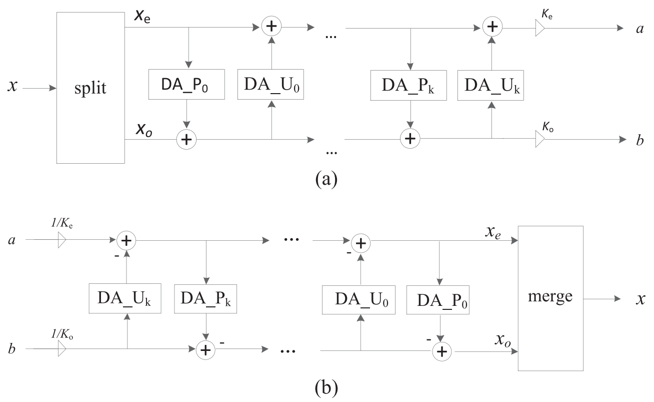

Fig. 1. Generic 1-D directional lifting wavelet transform. (a) Forward decomposition. (b) Reverse synthesis.

the odd sample subset x_o

$$\begin{cases} x_e\,[m,n] = x\,[2m,n] \\ x_o\,[m,n] = x\,[2m+1,n]. \end{cases} \tag{1}$$

In the predict stage, the odd elements are predicted by the neighboring even elements with a prediction direction, which was obtained by discriminant criteria. Suppose the direction adaptive prediction operator is DA_P, then the predict process can be represented as

$$d\,[m,n] = x_o\,[m,n] + DA\_P_e\,[m,n]\,. \tag{2}$$

In the update stage, the even elements are updated by the neighboring prediction error with the same direction of the predict stage. Suppose the direction adaptive update operator is DA_U, the updated process can be described as

$$c\,[m,n] = x_e\,[m,n] + DA\_U_d\,[m,n]\,. \tag{3}$$

Here, the directional prediction operator DA_P is

$$DA\_P_e\,[m,n] = \sum_i p_i x_e\,[m + sign(i-1)\tan\theta_v, n+i]. \tag{4}$$

The directional update operator DA_U is

$$DA\_U_d\,[m,n] = \sum_j u_j d\,[m + sign(j)\tan\theta_v, n+j]. \tag{5}$$

p_i and u_j are the coefficients of high pass filter and low pass filter, respectively. θ_v represents the direction of prediction and update.

Finally, the outputs of the lifting are weighted by coefficients K_e and K_o, which normalize the scaling and wavelet functions, respectively.

For a remote sensing image, if the directional lifting is performed along the direction of edge and texture, then more energy of the image will be concentrated in low-frequency subband, which is beneficial to improve the coding performance. Chang and Girod [23] provide a set of reference directions for the adaptive directional lifting (ADL)-based wavelet transform, which only uses some integer pixels. Although it is simple and easy to implement, the optional directions are too sparse to present the rich directional information of the remote sensing image. Conversely, Ding *et al.* [22] just uses the proximal fractional pixels as the reference directions and fails to utilize the correlation with the distal integer pixels. For remote sensing images, obviously, the more the reference directions, the more accurate the description of its detail information. However, the side information will also increase. In this paper, the integer pixels and fractional pixels, which close to the predicted pixel, are considered. The set of reference directions of the horizontal transform and vertical transform are shown in Fig. 2(a) and (b), respectively. For each transform, i.e., the horizontal transform or vertical transform, 15 reference directions are chosen for direction lifting, which exploit some adjacent integer pixels or fractional pixels. In Fig. 2(a), the horizontal transform is performed on those black pixels, which need to utilize the white pixels of

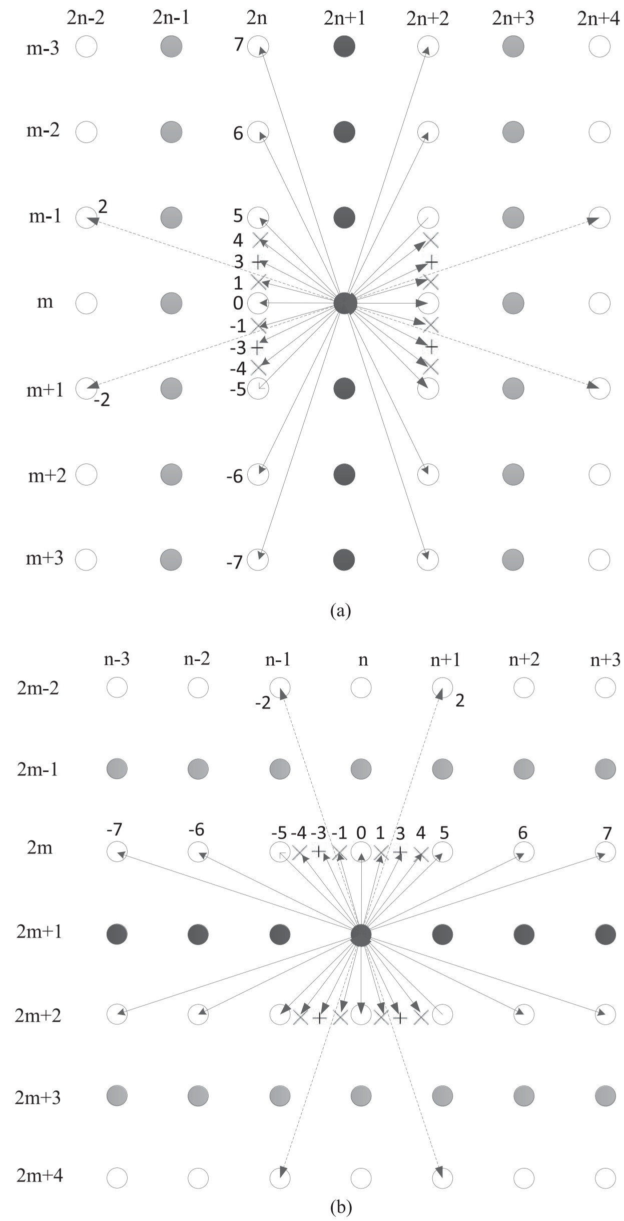

Fig. 2. Reference direction set of the directional lifting-based wavelet transform. (a) Horizontal transform. (b) Vertical transform.

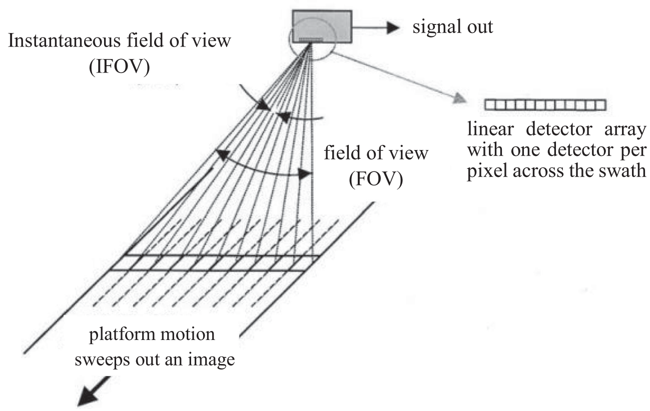

Fig. 3. Image formation by a "push-broom" mechanism.

adjacent columns and interpolate them. The closer the distance, the larger the pixel correlation. Therefore, more positions adjacent to the transformed pixel are chosen as lifting directions. In Fig. 2(a), we record the lifting direction set as [–7, –6, –5, –4, –3, –2, –1, 0, 1, 2, 3, 4, 5, 6, 7]. For the direction set, the "positive" represents the directions above the pixel to be lifting, and the "negative" represents that below the pixel to be lifting. "4," "3," and "1" represent the direction of fractional pixels at the $1/4$, $1/2$, and $3/4$ positions, respectively. "7," "6," "5," "2," and "0" represent those directions with different integer pixels. It can be seen that the traditional 2-D wavelet transform is a special case of the directional lifting wavelet transform in "0" direction. The process of vertical transform is similar to that of the horizontal transform.

B. Image Segmentation

In order to ensure the consistency of lifting direction and the local orientation of an image, image segmentation is usually performed first. The segmentation method based on rate-distortion optimization is proven to be a very efficient method for natural images [22]. It divides an image recursively into blocks with different sizes by quadtree. However, remote sensing images are usually recorded by a spaceborne or airborne imaging equipment with a large FOV. The imaging process of remote sensing images with a "push-broom" mechanism is shown in Fig. 3. The imaging technologies utilized in satellite programs usually record images by moving the FOV of the instrument across the earth's surface. The forward motion of the satellite can allow the subsequent pixels to be recorded along the satellite travel direction in the manner [31]. The FOV of a sensor corresponds to the width of the image (swath width). Take some commonly used sensors, for example, the Ikonos's FOV is 11.3 km, the QuickBird's FOV of is 16.5 km, and the SPOT-5's FOV of is 60 km [32]. Therefore, a remote sensing image usually covers a large range of geomorphology, which usually contains a lot of ground objects, except for a few special scenes such as deserts or still water. As a result, remote sensing images usually are of low spatial redundancy, especially for the high spatial resolution remote sensing image. In this situation, the segmentation performance based on rate-distortion optimization will be greatly affected. The reason is that the characteristics of the remote sensing image make the segmentation results have a large probability that almost all the blocks are with the smallest size that is allowed. In other words, the results of adaptive segmentation are nearly equivalent to those based on the same size of blocks.

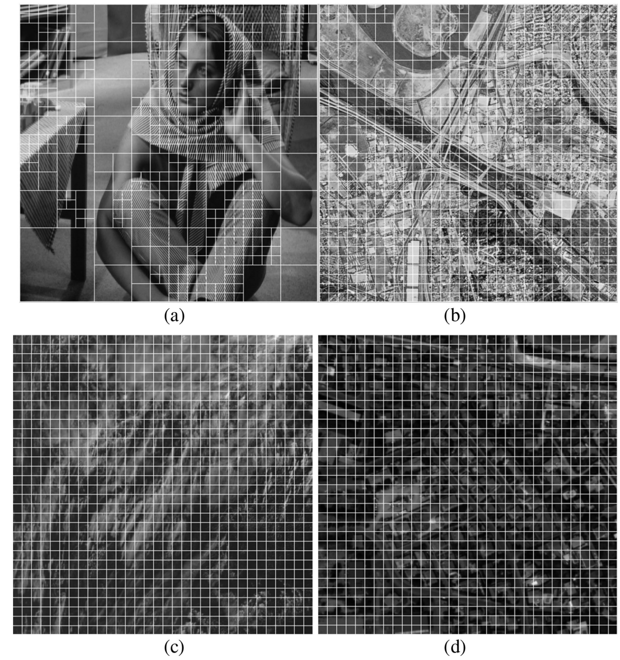

Fig. 4. Segmentation results with the adaptive segmentation method under the same condition. (a) A natural image "Barbara." (b) A remote sensing image "SanDiego" (8 b). (c) A remote sensing image "ocean_2kb1" (10 b). (d) A remote sensing image "pleiades_portdebouc_pan" (12 b).

Here, some experiments are performed on a natural image and three remote sensing images with an adaptive segmentation method, which the smallest size of a block is set to 16×16. The "SanDiego" has come from the USC-SIPI image database, whose bit depth is 8 b [33]. "ocean_2kb1" and "pleiades_portdebouc_pan" are derived from the CCSDS image set; their bit depth is 10 and 12 b, respectively [34]. These test remote sensing images reflect different geomorphic scenes, including city, ocean, and harbor. The segmentation results of these are shown in Fig. 4(a)–(d), respectively.

It can be seen in Fig. 4 that, compared with the natural image, large size blocks in remote sensing images are very rare. Especially for those remote sensing images with large bit depth, such as "ocean_2kb1" and "pleiades_portdebouc_pan," the results of segmentation are the minimum block that is allowed. With experiments on a larger set of remote sensing images, a similar conclusion can be obtained. It means that the adaptive segmentation method for remote sensing images is of little significance, and the complexity of the algorithm will be increased. In addition, if the adaptive segmentation method is used, the segmentation trees are also needed to be transmitted as the side information. For different bit rates, the segmentation trees are different, which makes the side information very heavy.

Because of its imaging mechanism, remote sensing images usually cover a large range of geomorphology, which makes the details of the image, such as geometric information, edge, and texture information, usually very abundant. In order to provide a good representation of remote sensing images, the segmented block should not be too large. On the other hand, the optimal lifting direction of each block should be preserved as the side information for image reconstruction. If the size of the image block is too small, there will be a lot of side information that needs to be stored, which will be a great burden to the compression. Therefore, the size of the segmented image block should be appropriate. With experiments on some remote sensing images with various complexities, we found that if the image block size is less than 16×16, sometimes the coding efficiency with the direction lifting wavelet is even worse than that of the traditional wavelet transform. The reason is that, at the same bit rate, the more the side information, the fewer the bits actually used to code. Therefore, in this paper, the image block size is set to 16×16.

Based on the above analysis, for remote sensing images, we adopt the block segmentation method with the same size directly. For a remote sensing image with size $M \times N$, those initial image blocks can be represented as $B_{i,j}$, $i = 1, 2, \ldots, M/16$, $j = 1, 2, \ldots, N/16$. After transformation, the size of the blocks depends on the decomposition level. Suppose the level of directional wavelet decomposition is J, for the k_{th} decomposition level, the size of the block can be represented as $L_k \times L_k$. That is

$$L_k = 16/2^{k-1},\ k = 1, 2, \ldots, J. \tag{6}$$

In other words, the size of the block is reduced to $1/4$ of the original size when one level of wavelet decomposition is carried out. Compared with the adaptive segmentation method based on rate-distortion optimization, the complexity of the segmentation method with the same size is greatly reduced. Furthermore, it does not need to transmit any side information.

C. Chosen of Optimal Prediction Direction

For the directional lifting wavelet transform, the prediction error is reflected in the high-frequency subbands. Obviously, the smaller the prediction error, the less the information in high-frequency subbands. As a result, the coding performance will be improved. Therefore, for a given block, the optimal prediction direction is the direction with minimal residual information in high-frequency subbands.

Suppose that the reference direction set is $\theta_{\mathrm{ref}} = [-7, -6, -5, -4, -3, -2, -1, 0, 1, 2, 3, 4, 5, 6, 7]$, and the total number of blocks is $N_a = MN/256$. For each block B_l, $l = 0, 1, \ldots, N_a - 1$, the optimal prediction direction θ^*_{opti} of it is calculated as follows:

$$\theta^*_{\mathrm{opti},B_l} = \underset{i \in \theta_{\mathrm{ref}}}{\operatorname{argmin}} \sum_{m,n \in B_l} D\left\{x(m,n) - DA\_P^i\left(x(m,n)\right)\right\}. \tag{7}$$

Here, $D(\cdot)$ represents the measure function of image distortion, and $x(m,n)$ represents the value at the position (m,n) in the block B_l. In this paper, let $D(\cdot) = |\cdot|$. It means that, for a given block B_l, the optimal prediction direction is the direction which is of minimal prediction error.

For an original image, the directional wavelet transform is conducted along all the given reference directions $\theta_{\mathrm{ref}}(\mathrm{ref} = 1, 2, \ldots, 15)$, respectively. Then, the optimal

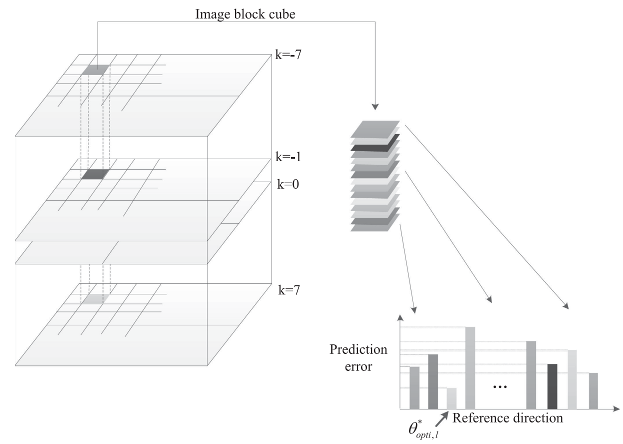

Fig. 5. Process of finding the optimal prediction direction of a block.

prediction direction of each block should be determined. The process of finding the optimal prediction direction of a block is shown in Fig. 5. For a given block B_l $(l = 0, 1, \ldots, N_a - 1)$, we calculate the prediction errors of the 15 "tiles," respectively. Then, we find the direction corresponding to the minimum prediction error, which is the optimal prediction direction $\theta^*_{\mathrm{ref},l}$ of this block. Repeat this process, until the optimal prediction directions of all blocks are determined. The optimal prediction direction set can be represented as $[\theta^*_{\mathrm{ref},0}, \theta^*_{\mathrm{ref},1}, \ldots, \theta^*_{\mathrm{ref},N_a-1}]$. For each block B_l, with the optimal prediction direction $\theta^*_{\mathrm{opti},\ l}$, the predicted process and the updated process of all elements of it are carried out by formula (2) and (3), respectively.

For the multi-level directional lifting wavelet transform, it exists close to dependencies among the blocks at the same position of each decomposition level. Some experiments that were performed on a large set of remote sensing images prove that, for the blocks at the same position of different decomposition levels, the optimal directions of them are very close, which means that these blocks have a great probability to choose the same reference prediction direction. Therefore, we only calculate the optimal lifting direction of each block in the first decomposition level, and the lifting directions of blocks in the other decompositions levels are the same as that in the first decomposition level. In this way, the complexity of the algorithm is greatly reduced. Moreover, the proposed direction lifting wavelet transform does not need to transmit the segmentation trees at different bit rates; it only needs to transmit the optimal prediction direction of each block as side information. The bit overhead of side information is analyzed as follows.

For the proposed directional wavelet transform, the optimal lifting directions of all blocks should be transmitted to the receiver as side information. Suppose that the size of the image is $M \times N$ and the block size is $P \times Q$. Then, the number of blocks is MN/PQ. Because the number of reference prediction directions is 15, we can use 4 b to represent the optimum prediction direction of each block. That means that a maximum of $(MN/PQ).4$ bits are required to store these directions. For reducing the side information, entropy coding can be used for encoding these bits. In this paper, as an effective coding method, Huffman coding is employed to encoding the direction information. Take the image "Barbara" in Fig. 4(b), for example, after entropy coding, the bit rate of side information is 0.0064 bpp. For the adaptive segmentation method introduced in [22], it needs different bit overhead at different bit rates. For "Barbara," the bit rate for coding the segmentation tree and associated directions at 0.125, 0.25, and 0.5 bpp is 0.008, 0.013, and 0.018 bpp, respectively. The advantage of the proposed method is more obvious in progressive image transmission, i.e., the proposed method only needs to transmit the side information once, and the adaptive segmentation method needs to transmit the side information at each bit rate.

D. Directional Adaptive Interpolation

For ADL-based wavelet transform, the sinc interpolation filter is commonly adopted. However, the sinc interpolation filter is performed only using the coefficients in the horizontal or vertical direction, which may blur the orientation property of the image and increase the directional prediction errors for those images with rich textures. For remote sensing images, it usually contains abundant texture and detail information. Therefore, the design of a directional interpolation filter is very important. Besides interpolation performance, another factor that needs to be considered is that side information generated by the directional interpolation filter should be reduced as much as possible due to the compression efficiency. The reason is that an optimal interpolation filter is usually closely related to the content of the image. In theory, the subpixel interpolation problem also can be seen as the design of an optimal interpolation filter. Since the interpolation filter can be classified as an FIR filter, one can design the filter to minimize the energy of the high-frequency subband

$$D = \sum_{m,n} |e(m,n)|^2 = \sum_{m,n} \left| x_o(m,n) - \sum_k a_k x(m,n+k) \right|^2. \tag{8}$$

The minimization problem

$$D = \min_{\ldots a_{k-1}, a_k, a_{k+1}, \ldots} \sum_{m,n} \left| x_o(m,n) - \sum_k a_k x(m,n+k) \right|^2 \tag{9}$$

is essentially a process of finding a set of optimal filter coefficients$\{\ldots, a_{k-1}, a_k, a_{k+1}, \ldots\}$. For a given image, the optimal interpolation filter coefficients have to be stored and sent to the decoder as side information. The more filter coefficients, the more side information that needs to be transmitted. Accordingly, the coding performance of the image will be greatly affected. Therefore, a good balance between interpolation performance and side information is an important issue, which needs to be solved. In this paper, an effective weighted directional interpolation filter is adopted [35]. The basic process of direction interpolation is shown in Fig. 6.

In Fig. 6, for different sub-pixel positions, some different integer pixels are used to interpolate the sub-pixel, and the interpolation direction is adapted to the properties of the signal for interpolation. For examle, in order to interpolate a quarter-position coefficient, not only the integer coefficients $\{c_{-2}, c_{-1}, c_0, c_1\}$ but also the coefficients $\{c_{-3}, c_2\}$ along the predicted direction are used. The directional interpolation filter should be constructed by these coefficients $\{c_{-3}, c_{-2}, c_{-1}, c_0, c_1, c_2\}$ in the integer position and make a prediction to the sub-pixel position. The final coefficients of directional interpolation filter are determined by three kinds of filters: bilinear filter, Telenor 4-tap filter, and 2-tap filter. The directional interpolation process is shown in Fig. 7. The coefficients of these filters are listed in Table I.

It can be seen from Fig. 7 that $\{c_{-3}, c_2\}$ are the inputs of the bilinear filter, $\{c_{-2}, c_{-1}, c_0, c_1\}$ are the inputs of the Telenor 4-tap filter, and both the output of the bilinear filter and the Telenor 4-tap filter are as the inputs of the 2-tap filter. As a result, the outputs of the 2-tap filter are the weighted coefficients of the directional interpolation filter. By this way, some directional

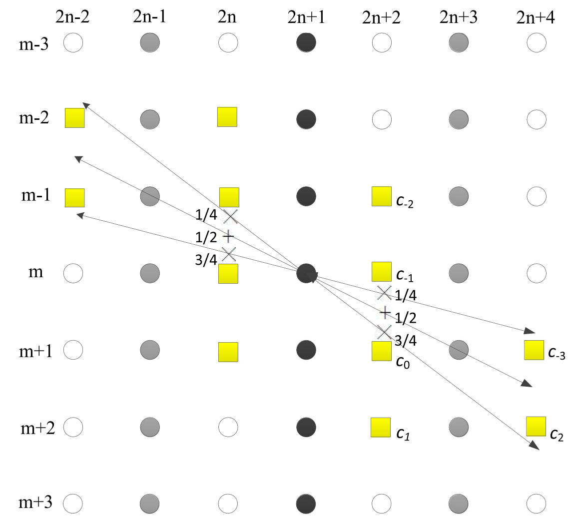

Fig. 6. Process of directional interpolation.

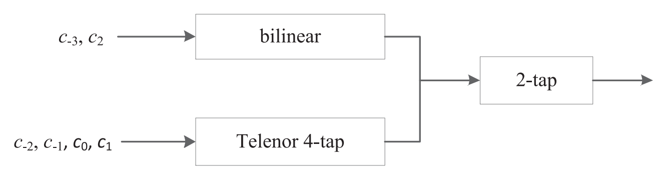

Fig. 7. Block diagram of directional interpolation.

TABLE I
APPLIED FILTERS OF DIRECTIONAL INTERPOLATION PROCESS

Filter	Position	The weights of filter
Bilinear filter	1/4	3/4; 1/4
	1/2	1/2; 1/2
	3/4	1/4; 3/4
Telenor 4-tap filter	1/4	-1/16; 13/16; 5/16; -1/16
	1/2	-1/8; 5/8; 5/8; -1/8
	3/4	-1/16; 5/16; 13/16; -1/16
2-tap filter	N/A	-1/4; 5/4

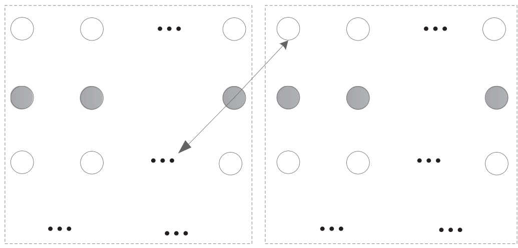

Fig. 8. Diagram of the processing of the block boundary.

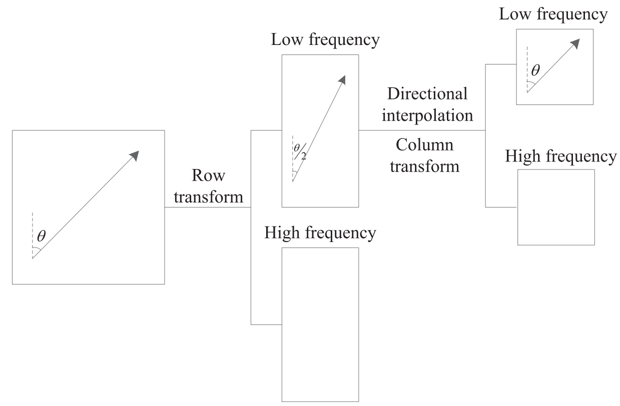

Fig. 9. Processing procedure of direction displacement for a block.

information of images can be preserved effectively, and no side information is needed to be sent.

E. Processing of Block Boundaries

A general principle for the process of block boundaries is that each block could only make use of its own direction information. However, it is very easy to produce boundary effects. In this paper, for the transform of pixels in block boundaries, the adjacent pixels of other blocks are used, unless the boundary pixels are at the edge of the image. The diagram of the processing of the block boundary is shown in Fig. 8. In Fig. 8, the dotted line represents the boundary of a block. As a result, blocking artifacts can be avoided although the block segmentation is carried out for direction detection.

F. Processing of Direction Deviation

The 2-D wavelet transform can be regarded as a combination of two 1-D transformations. Assuming that row transformation is performed first, then the size of the image block is changed, which makes the block direction no longer accurate. To solve the problem, some studies have tried to reduce the angle of the block to half and then perform another 1-D transform with the half-angle, such as in [36]. However, the half-angle may not be exactly as the optimal prediction direction that was calculated previously, which may lead to direction deviation. With the increase of the decomposition levels, the direction deviation will be accumulated. A solution that is easy to think is to calculate the optimal prediction direction of the "new" block again by traversing, but the complexity is high and the side information will be increased. For this problem, we adopt the directional interpolation method that was introduced in Section II–D to interpolate the rectangular block into a square block first, then another 1-D transform is performed with the optimal prediction direction calculated previously. For a block, the processing procedure of direction displacement is shown in Fig. 9.

III. Content-Based Coding Method for Remote Sensing Images

In order to obtain good coding performance, image representation methods are usually combined with JPEG2000. However, the good performance of JPEG2000 is at the cost of high complexity. Some sophisticated components of it are the main contributors to the high coding performance. On the other hand, JPEG2000 is a general compression method, which is designed without considering the characteristics of remote sensing images. In this paper, a simple and efficient coding method is proposed, which is specially designed for remote sensing images. After the OADL-based wavelet transform, the energy of remote sensing images is more concentrated, which usually "enlarge" the difference among subbands due to the content of images. In this case, different scanning and coding methods will have a great impact on the compression performance. Therefore, a BTCCA is introduced, which can provide different scanning orders and scanning methods among and within subbands based on the content of images, and can encode more significant coefficients at the same bit rate. The proposed BTCCA algorithm is described in detail below.

A. Content-Based Adaptive Scanning Method

For a remote sensing image X with size $M \times N$, after the OADL-based wavelet transform, the transformed image can be recorded as Y. The process of scanning the transformed image can be regarded as a bijection f from a closed interval $[1, 2, \ldots, M \times N]$ to the set of ordered pairs $\{(i, j) : 1 \leq i \leq M, 1 \leq j \leq N\}$, where the latter set represents the locations of the image. After scanning, the 2-D transformed image can be converted to a 1-D coefficient sequence that can be represented as $[Y_{f(1)}, Y_{f(2)}, \ldots, Y_{f(MN)}]$. In fact, various scanning strategies are bijective functions f that are of different definitions. If the bijective function f is defined, then the process of compressing a transformed image becomes a process of compressing a 1-D coefficient sequence $\tilde{Y} = [Y_{f(1)}, Y_{f(2)}, \ldots, Y_{f(MN)}]$.

For a transformed image, the coefficients that are scanned first are encoded in priority, which leads to the codestream of these coefficients in front of the entire codestream. Accordingly, this part of the codestream will be decoded in priority and displayed if necessary. Therefore, at the same bit rate, different scanning order can lead to different quality of the reconstructed image, which makes the scanning order very important [38]. There are some commonly used scanning methods, such as raster scan, zigzag scan, and Morton scan. However, they do not take the characteristics of wavelet subband into consideration. More importantly, remote sensing images usually contain a great number of ground objects, which makes some information still remain in high-frequency subbands after the directional wavelet transform. According to different landforms recorded by remote sensing images, the amount of information of these subbands may be quite different. If a fixed scanning method is adopted, it does not guarantee that the scan is carried out according to the importance of the subbands. In other words, the subbands that scanned first may be less informational. Therefore, how to design an effective adaptive scanning method is also an important issue for improving the coding performance of the remote sensing image.

In this paper, an adaptive scanning scheme proposed by us previously is adopted [37]. The adaptive scanning scheme determines the scanning method and scanning order of wavelet subbands based on the image content. The algorithm of the content-based adaptive scanning method (CAS) is shown in *function CAS*.

function $S = CAS(X, J)$

Input: The wavelet transformed image X with OADL, the level of decomposition is J.

- Calculate the energy of each subband and represent it as $E_{\lambda,\theta}$. λ-Scale ($m = 1, 2, \ldots, J$), θ-Direction ($d = 1, 2, 3, 4$). "1" represents the lowest-frequency subband, "2" represents the horizontal direction, "3" represents the diagonal direction, and "4" represents the vertical direction, respectively.

$$E_{\lambda,\theta} = \frac{1}{RC} \sum_{i,j}^{R,C} X(\lambda, \theta)(i, j)^2$$

R and C are the number of rows and columns of the current subband $X(\lambda, \theta)$, respectively; $X(\lambda, \theta)(i, j)$ represents the coefficient of the current subband located in (i, j).

- Determine the scanning order among all the subbands according to their energy.
- **For** each subband $X(\lambda, \theta)$
  - If the subband is the lowest-frequency subband or horizontal subband, the "horizontal z-scan" is adopted.
  - If the direction of the subband is vertical, the "vertical z-scan" is exploited.
  - If the direction of the subband is diagonal, then the scanning method depends on the horizontal subband and vertical subband of this level.
    ① If $E_{\lambda,2} \geq E_{\lambda,4}$, the "horizontal z-scan" is performed to this subband.
    ② If $E_{\lambda,2} < E_{\lambda,4}$, the "vertical z-scan" is performed to this subband.

End

Output: The generated 1-D coefficient sequence S by scanning the 2-D transformed image X.

It has been demonstrated that from the CAS algorithm, the adaptive scanning method is performed by two steps. First, after the directional wavelet transform, the energy of each subband is calculated, and the scanning order among subbands is determined by their energy in descending order. Second, for the scan

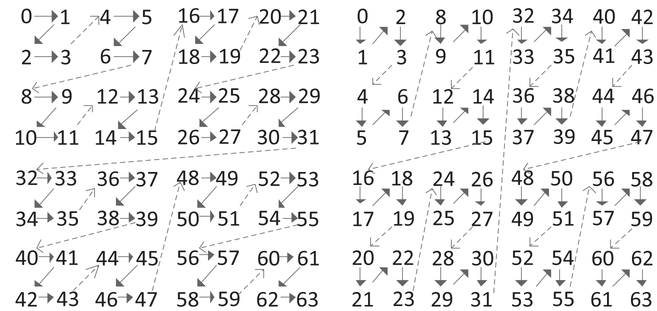

(a) (b)

Fig. 10. "Horizontal z-scan" method and "vertical z-scan" method. (a) The "horizontal z-scan" method is used for the subbands that contain more horizontal information. (b) The "vertical z-scan" method is used for the subbands that contain more vertical information.

within a subband, the scanning method is determined by the characteristic of the subband. The "horizontal z-scan" method and the "vertical z-scan" method are shown in Fig. 10.

B. Binary Tree Codec With Content-Based Adaptive Scanning (BTCCA)

The embedded coding methods based on quadtree are commonly used. However, Shaffer *et al.* [38] pointed out that the coding method based on binary tree decomposition is more efficient and simpler than that based on quadtree decomposition. Inspired by recent advancements in the binary tree coding technique proposed in [39], we propose a BTCCA method combining the binary tree codec with the content-based adaptive scanning method. The BTCCA algorithm is as follows.

function $\text{code} = BTCCA(X, J, T_k)$

Input: X represents the transformed image with OADL-based wavelet transform, J is the level of wavelet decomposition, T_k is the current threshold.

Initialization:

- $S = CAS(X, J)$
- Establish a binary tree Γ by the 1-D coefficient sequence S.
- $d = D$.

While ($d > 1$)

{

- For $i = \sum_{j=0}^{d-1} 2^j + 1 \ to \ \sum_{j=0}^{d} 2^j$
- Let $ct = \{\ \}$. If $\Gamma(i) \geq T_{k-1}$

If $\Gamma(i)$ is on the left of its brother, then
$ct = BTC(\Gamma, i+1, T_k)$;
Else
$ct = BTC(\Gamma, i-1, T_k)$.

- $\text{code} = \{\text{code}, ct\}$.
- $d = d - 1$.

Output: The codestream of the bit plane for the given threshold T_k.

}

function code $= BTC(\Gamma, i, T_k)$

Input: Γ represents a binary tree, and is the index of a node of the binary tree. T_k represents the threshold. $T_0 = 2^{\lfloor \log_2 \Gamma(1) \rfloor}$, and $T_k = T_0/2^k$.

- If $\Gamma(i)$ has been coded with significant in a larger threshold, i.e., $\Gamma(i) \geq T_{k-1}$, then
  If $\Gamma(i)$ is not in the bottom level of the binary tree, code the two children of $\Gamma(i)$, else the sign of $\Gamma(i)$ is coded.
- If $\Gamma(i)$ has a significant parent, and the brother of $\Gamma(i)$ is insignificant, then
  If $\Gamma(i)$ is not in the bottom level of the binary tree, code the two children of $\Gamma(i)$, else the sign of $\Gamma(i)$ is coded.
- If $\Gamma(i) \geq T_k$
  If $\Gamma(i)$ is not in the bottom level of the binary tree, code the two children of $\Gamma(i)$, and add a "1" before the codestream. Else the sign of $\Gamma(i)$ is coded, and add a "1" before the codestream.
- Else
  "0" is output.

Output: The codestream of the subtree whose root is the node $\Gamma(i)$.

For the BTCCA algorithm, after the OADL-based wavelet transform, the CAS method is utilized to the transformed image first, and a 1-D coefficient sequence is obtained. Second, a binary tree is established based on the 1-D coefficient sequence by comparing the two adjacent coefficients in turn. Following, for each level of the binary tree, the binary tree coding algorithm is carried out at a given threshold.

IV. Quality Evaluation Index

In order to evaluate the proposed compression method comprehensively, peak signal-to-noise ratio (PSNR, dB), kappa coefficient, and multi-scale structural similarity method (MS-SSIM) are chosen as the evaluation indexes, respectively.

A. Peak Signal-to-Noise Ratio

Suppose X and Y are the original image and the reconstructed image, respectively. L represents the possible maximum value of the original image. The PSNR can be calculated as follows.

$$\mathrm{PSNR} = 10 \log_{10} \frac{L^2}{\|X - Y\|_2}. \tag{10}$$

B. Kappa Coefficient

Kappa coefficients are widely used as the classification accuracy assessment for remote sensing images [40]. Cohen [41] points out that the kappa coefficient can be utilized as a measure of agreement between the original and the decoded images. In this case, the pixels of the original image are seen as reference data (observations), and the pixel of the decoded image are seen as classified data. The kappa coefficient is defined as

$$\hat{K} = \frac{N \sum_{i=1}^{c} x_{ii} - \sum_{i=1}^{c} (x_{i+} \cdot x_{+i})}{N^2 - \sum_{i=1}^{c} (x_{i+} \cdot x_{+i})}. \tag{11}$$

Here, N is the total number of observations, c represents the number of rows of the confusion matrix, x_{ii} represents the number of observations in row i and column i, and x_{i+} and x_{+i} are the marginal totals of row i and column i, respectively.

C. Multi-Scale Structural Similarity Method (MS-SSIM)

The MS-SSIM is a multi-scale structural similarity method that incorporates the variations of viewing conditions and more flexible than SSIM [42]. Thus, we adopt the MS-SSIM as an evaluation index in this paper.

$$\mathrm{MS\_SSIM}(x, y) = [l_M(x, y)]^{\alpha_M} \cdot \prod_{j=1}^{M} \left[c_j(x, y)^{\beta_j} s_j(x, y)^{\gamma_j} \right]. \tag{12}$$

Here, $l(x, y)$, $c(x, y)$, and $s(x, y)$ represent the luminance, contrast, and structure comparison, respectively.

V. Experiments and Results

In this section, some experiments are implemented to verify the effectiveness of the proposed compression method for remote sensing images. The proposed compression method is compared with other five scan-based compression methods, i.e., SPIHT, SPECK, CCSDS, JPEG2000, and BTCA, in terms of some evaluation indexes at different bit rates. First, in order to compare the visual quality of reconstructed images obtained by the proposed compression method and that obtained by other compression methods, the "Pentagon" and "North Island" are chosen as test images. In the experiments, the level of wavelet decomposition is set to five. The comparison results of reconstructed images obtained by different compression methods at 0.0313 and 0.0625bpp are shown in Figs. 11 and 12, respectively.

In Figs. 11 and 12, we can observe that the visual quality of reconstructed images obtained by the proposed compression method is better than that of other compression methods at the same bit rate. This advantage is particularly evident for the box area. The reason is that the OADL model provides a more efficient representation of the image, which helps to preserve more details of an image. Moreover, the BTCCA coding method ensures that more significant coefficients are scanned and encoded in priority, especially the coefficients at the edge of the image. As a result, at the same bit rate, the proposed compression method can provide better visual quality of the reconstructed image. For other four methods, visual quality of the reconstructed image obtained by CCSDS is the worst. One reason is that CCSDS set the decomposition level to three, so the coding performance is limited. Another important reason is that CCSDS divides the transformed image into some blocks and then divides the block set into several segments. The number of blocks in a segment can be 16 to 220, and these blocks are continuous in the raster order. Each segment is encoded separately and is not relevant to the other segments. Therefore, the reconstructed images of

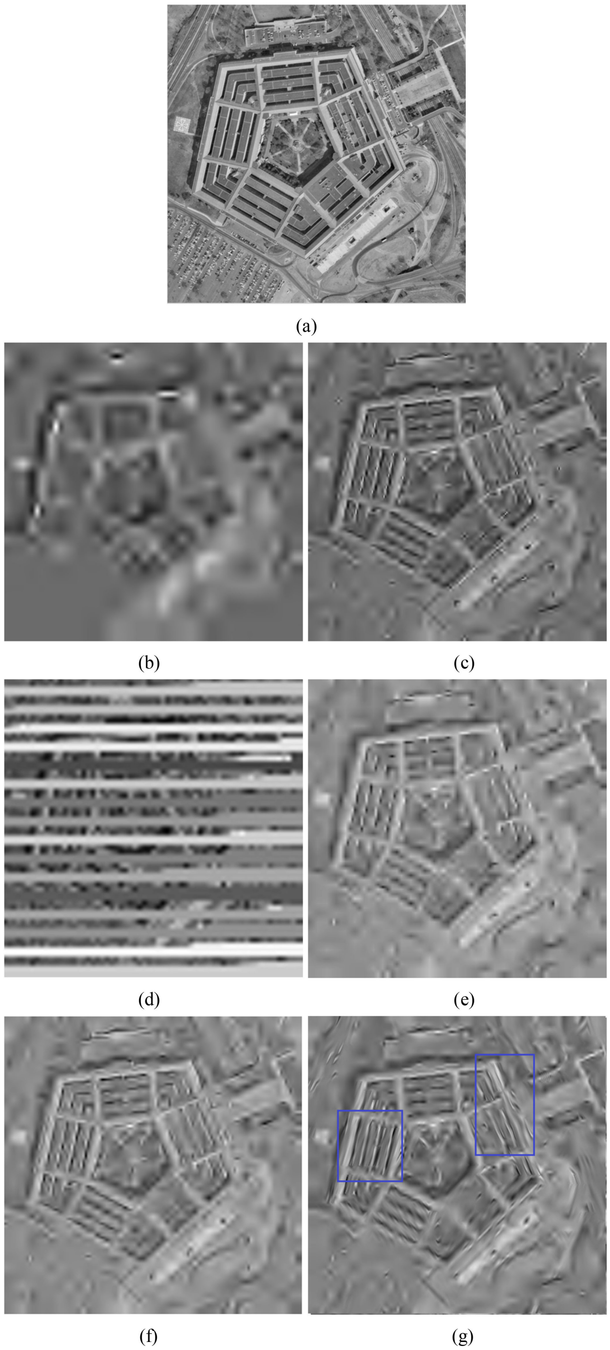

Fig. 11. Comparison of visual quality of reconstructed images obtained by the proposed compression method and other scan-based compression methods at 0.0313 bpp. (a) Original image "Pentagon." (b) Reconstructed image obtained by SPIHT. (c) Reconstructed image obtained by SPECK. (d) Reconstructed image obtained by CCSDS. (e) Reconstructed image obtained by JPEG2000. (f) Reconstructed image obtained by BTCA. (g) Reconstructed image obtained by the proposed method.

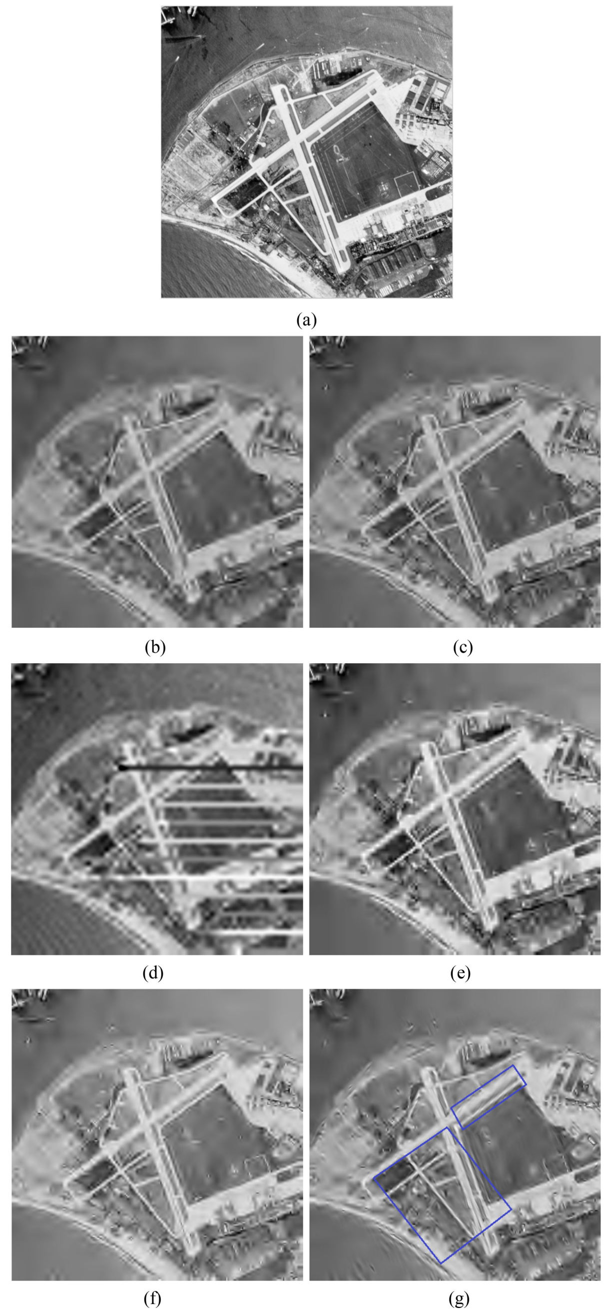

Fig. 12. Comparison of visual quality of reconstructed images obtained by the proposed compression method and other scan-based compression methods at 0.0625 bpp. (a) Original image"North Island." (b) Reconstructed image obtained by SPIHT. (c) Reconstructed image obtained by SPECK. (d) Reconstructed image obtained by CCSDS. (e) Reconstructed image obtained by JPEG2000. (f) Reconstructed image obtained by BTCA. (g) Reconstructed image obtained by the proposed method.

CCSDS are prone to stripe effects, especially at very low bit rates.

Here, the proposed method is compared with other compression methods from the perspective of mean square error (MSE). In order to better display the comparison results, we use SNR instead of PSNR. For the image "Pentagon" and "North Island," the SNR results of different methods at different bit rates are shown in Fig. 13(a) and (b), respectively. The range of bit rate is from 0.1 to 1 bpp. In Fig. 13, it can be seen that the proposed method consistently exceeds that of other scan-based compression algorithms.

In order to evaluate the proposed compression method comprehensively, more experiments are performed from the perspective of objective evaluation. The test image set includes four test remote sensing images. The two images are "Pentagon"

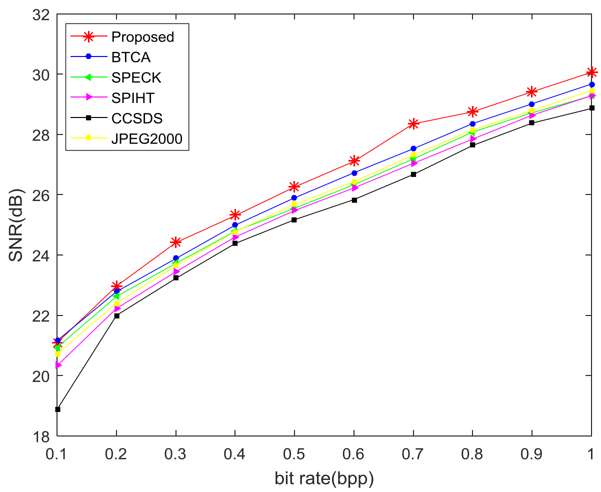

(a)

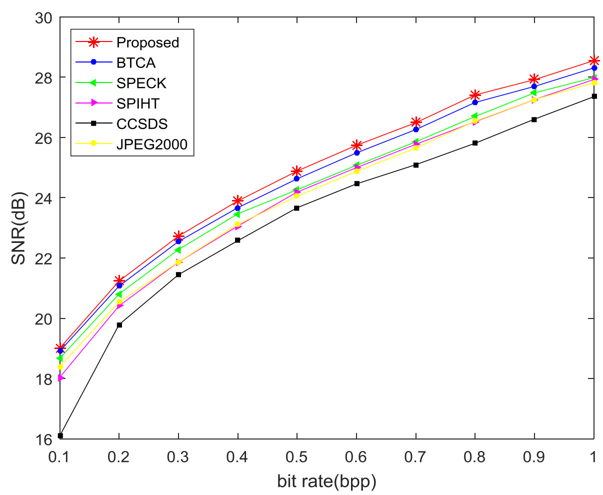

(b)

Fig. 13. Comparison of rate-distortion performance between 0.1–1 bpp for different test images. (a) "Pentagon." (b) "North Island."

(a)

(b)

Fig. 14. Part of the test remote sensing images used in the experiment. (a) San Diego1 (Miramar NAS). (b) San Diego2 (Miramar NAS).

and "North Island," which are shown in Figs. 11(a) and 12(a), respectively. And the other two images are shown in Fig. 14. All the test images are derived from the USC-SIPI database [33], which reflect different geomorphological scenes, including ridge, pentagon, island, and urban. The size of these images is 512×512.

In the experiments, the level of wavelet decomposition is set to five. All these test images are compressed by the proposed OADL-based compression methods and the other scan-based method, respectively. For the proposed method, the side information of the four test images is 0.00815, 0.00963, 0.00937, and 0.00716 bpp, respectively. The comparison results of PSNRs, kappa coefficients, and MS-SSIMs of these compression methods are tabulated in Table II, Table III, and Table IV, respectively, Tables V–VII, and The results are evaluated at six bit rates, namely, 0.0313, 0.0625, 0.125, 0.25, 0.5, and 1 bpp.

In Table II, the comparison results are listed from the perspective of MSE. We can observe that, for these compression algorithms, the PSNRs of CCSDS are low. The reason is that CCSDS is designed for on-board compression; the complexity of the algorithm is an important issue that must be considered. Moreover, for CCSDS, the level of the wavelet decomposition is fixed to three, which also limits its coding performance to some extent, especially at low bit rates. Compared with SPIHT, the encoding process of SPECK does not utilize the offspring relation of the spatial direction trees. Instead, it encodes each image block independently, which makes it more fault-tolerant and thus obtains good PSNRs. The PSNR results of JPEG2000 are higher than those of SPIHT, because the complicated models of JPEG2000, including the encoding stages (tier-1 and tier-2 coding), context model, and post-compression rate-distortion optimization, are all contributed to the improvement of coding performance. For BTCA, the coding process based on binary tree decomposition is very effective, which traverses a binary tree by an adaptive way, and can provide an excellent coding performance. The proposed compression method achieves the highest coding performance. The reason is that, for remote sensing images, the designed OADL method can provide a more efficient representation of the image, which is beneficial to improve the coding performance. In addition, during the process of coding, a content-based adaptive scanning method is adopted, which takes the scanning order among subbands and the scanning strategy within a subband into consideration simultaneously, and ensures that much more important coefficients can be scanned in priority. Hence, at the same bit rate, the proposed compression method can provide better compression performance.

Table III provides the comparison results from the perspective of structural similarity. The MS-SSIM evaluates the similarity between the original image and the reconstructed image in a more flexible way. From Table III, we observe that the MS-SSIM results of the proposed compression method consistently exceed that of other scan-based algorithms at all given bit rates. The reason is that, for the proposed method, the OADL model can provide a better representation of the detail information of remote sensing images. Moreover, during the process of coding, the proposed method also encodes the brothers of those edge coefficients based on the fact that the magnitudes of the coefficients around the edges are often large too. As a result, more texture and contour information of remote sensing images can be preserved by using the proposed method, which helps to improve the structural information of the reconstructed image.

TABLE II
PSNRs (dB) OF THE PROPOSED COMPRESSION METHOD AND OTHER SCAN-BASED COMPRESSION METHODS

Image	0.0313bpp						0.0625bpp					
	SPIHT	SPECK	CCSDS	J2K	BTCA	Proposed	SPIHT	SPECK	CCSDS	J2K	BTCA	Proposed
SanDiego1	18.53	20.12	12.30	19.67	20.17	**20.20**	20.44	21.23	16.83	20.81	21.28	**21.38**
Pentagon	21.59	23.80	14.05	23.32	23.82	**23.86**	24.10	25.13	21.01	24.83	25.26	**25.36**
NorthIsland	19.07	21.40	12.07,	20.97	21.55	**21.73**	21.82	23.01	17.93	22.68	23.16	**23.28**
SanDiego2	19.40	21.31	11.60	20.86	21.38	**21.46**	21.71	22.24	18.45	22.33	22.52	**22.67**
Image	0.125bpp						0.25bpp					
	SPIHT	SPECK	CCSDS	J2K	BTCA	Proposed	SPIHT	SPECK	CCSDS	J2K	BTCA	Proposed
SanDiego1	22.26	22.77	21.62	22.54	22.87	**22.98**	24.31	24.65	24.21	24.50	24.78	**24.91**
Pentagon	26.03	26.62	25.41	26.39	26.71	**26.87**	28.01	28.42	27.82	28.20	28.55	**28.77**
NorthIsland	24.18	24.82	23.08	24.41	25.05	**25.16**	26.76	27.02	26.26	26.81	27.36	**27.57**
SanDiego2	23.55	24.04	23.15	23.61	24.16	**24.29**	25.52	25.78	25.44	25.65	25.95	**26.08**
Image	0.5bpp						1 bpp					
	SPIHT	SPECK	CCSDS	J2K	BTCA	Proposed	SPIHT	SPECK	CCSDS	J2K	BTCA	Proposed
SanDiego1	26.72	26.93	26.71	26.80	27.12	**27.56**	29.92	29.95	29.81	29.97	30.33	**30.46**
Pentagon	30.63	30.71	30.33	30.84	31.06	**31.41**	34.44	34.44	34.02	34.62	34.83	**35.22**
NorthIsland	29.70	29.78	29.18	29.56	30.14	**30.40**	33.44	33.50	32.87	33.32	33.82	**34.06**
SanDiego2	27.86	28.11	27.83	27.93	28.22	**28.29**	30.96	31.14	30.79	31.10	31.30	**31.36**

TABLE III
PSNRs (dB) OF THE PROPOSED COMPRESSION METHOD AND OTHER SCAN-BASED COMPRESSION METHODS

Image	0.0313bpp						0.0625bpp					
	SPIHT	SPECK	CCSDS	J2K	BTCA	Proposed	SPIHT	SPECK	CCSDS	J2K	BTCA	Proposed
SanDiego1	0.4700	0.6675	0.2877	0.6242	0.6679	**0.6694**	0.7021	0.7697	0.5683	0.7395	0.7726	**0.7783**
Pentagon	0.4645	0.7273	0.2433	0.6811	0.7293	**0.7380**	0.7390	0.8266	0.6486	0.8039	0.8252	**0.8367**
NorthIsland	0.5689	0.7467	0.3066	0.7174	0.7450	**0.7558**	0.7654	0.8152	0.6546	0.8076	0.8193	**0.8244**
SanDiego2	0.5026	0.6916	0.2402	0.6616	0.6917	**0.6966**	0.7202	0.7542	0.6569	0.7663	0.7821	**0.7879**
Image	0.125bpp						0.25bpp					
	SPIHT	SPECK	CCSDS	J2K	BTCA	Proposed	SPIHT	SPECK	CCSDS	J2K	BTCA	Proposed
SanDiego1	0.8339	0.8687	0.8008	0.8506	0.8680	**0.8712**	0.9120	0.9263	0.9148	0.9222	0.9250	**0.9286**
Pentagon	0.8659	0.8911	0.8429	0.8863	0.8913	**0.8993**	0.9318	0.9428	0.9320	0.9410	0.9433	**0.9456**
NorthIsland	0.8675	0.8876	0.8504	0.8697	0.8902	**0.8917**	0.9263	0.9377	0.9276	0.9296	0.9342	**0.9388**
SanDiego2	0.8373	0.8681	0.8246	0.8457	0.8682	**0.8745**	0.9143	0.9284	0.9132	0.9196	0.9268	**0.9338**
Image	0.5bpp						1 bpp					
	SPIHT	SPECK	CCSDS	J2K	BTCA	Proposed	SPIHT	SPECK	CCSDS	J2K	BTCA	Proposed
SanDiego1	0.9597	0.9627	0.9627	0.9638	0.9634	**0.9666**	0.9840	0.9852	0.9848	0.9850	0.9857	**0.9868**
Pentagon	0.9687	0.9734	0.9681	0.9663	0.9718	**0.9740**	0.9877	0.9881	0.9875	0.9870	0.9887	**0.9896**
NorthIsland	0.9611	0.9631	0.9638	0.9626	0.9640	**0.9670**	0.9831	0.9841	0.9850	0.9835	0.9845	**0.9855**
SanDiego2	0.9582	0.9642	0.9595	0.9628	0.9630	**0.9659**	0.9825	0.9837	0.9835	0.9842	0.9839	**0.9851**

TABLE IV
PSNRs (dB) OF THE PROPOSED COMPRESSION METHOD AND OTHER SCAN-BASED COMPRESSION METHODS

Image	0.0313bpp						0.0625bpp					
	SPIHT	SPECK	CCSDS	J2K	BTCA	Proposed	SPIHT	SPECK	CCSDS	J2K	BTCA	Proposed
SanDiego1	0.75%	1.18%	0.52%	1.04%	1.18%	**1.20%**	1.27%	1.38%	1.09%	1.30%	1.38%	**1.44%**
Pentagon	0.88%	1.66%	0. 43%	1.62%	1.65%	**1.70%**	1.79%	2.50%	1.82%	2.23%	2.47%	**2.62%**
NorthIsland	1.53%	2.23%	0.79%	2.09%	2.18%	**2.29%**	2.29%	2.63%	1.97%	2.57%	2.61%	**2.77%**
SanDiego2	0.95%	1.35%	0.50%	1.33%	1.41%	**1.47%**	1.53%	1.65%	1.42%	1.72%	1.78%	**1.85%**
Image	0.125bpp						0.25bpp					
	SPIHT	SPECK	CCSDS	J2K	BTCA	Proposed	SPIHT	SPECK	CCSDS	J2K	BTCA	Proposed
SanDiego1	1.76%	1.89%	1.74%	1.84%	1.90%	**1.95%**	2.33%	2.56%	2.41%	2.48%	2.54%	**2.62%**
Pentagon	2.70%	3.14%	2.82%	3.06%	3.00%	**3.26%**	3.81%	3.93%	4.04%	4.07%	3.94%	**4.22%**
NorthIsland	2.95%	3.11%	2.98%	3.05%	3.14%	**3.28%**	3.80%	4.02%	3.89%	3.89%	3.98%	**4.12%**
SanDiego2	2.05%	2.19%	2.05%	2.12%	2.24%	**2.31%**	2.77%	2.98%	2.75%	2.76%	2.93%	**3.00%**
Image	0.5bpp						1 bpp					
	SPIHT	SPECK	CCSDS	J2K	BTCA	Proposed	SPIHT	SPECK	CCSDS	J2K	BTCA	Proposed
SanDiego1	3.16%	3.25%	3.45%	3.40%	3.31%	**3.48%**	4.84%	4.78%	5.05%	4.96%	4.89%	**5.09%**
Pentagon	5.31%	5.44%	5.50%	5.34%	5.61%	**5.99%**	8.03%	8.27%	8.45%	8.35%	8.52%	**9.03%**
NorthIsland	4.98%	5.26%	5.09%	5.07%	5.30%	**5.48%**	7.45%	7.56%	7.60%	7.43%	7.72%	**8.02%**
SanDiego2	3.69%	3.81%	3.75%	3.78%	3.78%	**3.83%**	5.24%	5.30%	5.49%	5.51%	5.49%	**5.53%**

Table IV lists the comparison results of the kappa coefficient. The kappa coefficient is utilized here as a measure that evaluates the agreement between the original image and decoded image from the perspective of KHAT statistic. It can be seen in Table IV that the image decoding accuracy of the proposed compression method is still better than that of other five methods at all given bit rates.

Based on the analysis above, we can conclude that compared with other scan-based methods, the proposed compression method can provide a better coding performance. Moreover, it also works well when the bit rate is very low.

In order to further prove the effectiveness of the proposed compression method, a larger test image set is adopted for evaluating the compression performance. Here, 20 images from the CCSDS reference image set are used [34]. Among of them, 11 images with 8-b depth, including "marstest," "lunar," and all images of "coastal"; six images with 10-b depth, including "ice-2kb1," "ice-2kb4," "india-2kb1," "india-2kb4," "ocean-2kb1," and "ocean-2kb4; two images with 10-b depth, including "solar" and "sun_spot"; one image with 16-b depth, including "sar_16bit." These test images are of different sizes, six images with 512×512, seven images with 1024×1024, and seven images with 2048×2048, respectively. Table XI lists average PSNR, average MS-SSIM, and average kappa coefficient for all the test images of different methods at six bit rates.

From Table V, we can see that, compared with other compression methods, the average PSNRs of the proposed compared method are the highest at different bit rates. From the perspective of MS-SSIM, the proposed method is still the best. The reason is that the OADL model can provide a good representation of the direction information of an image. In addition, the proposed coding method can encode more significant coefficients at the same bit rate. Therefore, the reconstructed images obtained by the proposed method are of good quality. For the criterion of Kappa coefficient, similar results are obtained. Moreover, from the results of the proposed method (OADL only) and the proposed method (BTTCA only), we can see that the BTTCA module can improve the coding gain to some extent, and the OADL module provides most of the coding gain. From the perspective of image coding, a good image representation method ensures that more energy of the image can be concentrated in the low-frequency subband, which is also beneficial to the subsequent coding process. Therefore, combining the effective image representation module with the image coding module can improve the overall coding efficiency more effectively.

VI. Conclusion and Discussion

In this paper, an efficient compression method is proposed for remote sensing images. We first propose an OADL model, which calculates the optimal lifting direction of each image block, and the weighted directional adaptive interpolation is utilized in the process of lifting for preserving more directional characteristics of remote sensing images. Following, a BTCCA method is designed, which can scan a transformed image adaptively based on its content, and can encode more significant coefficients at

TABLE V
AVERAGE EVALUATION INDEXES OF THE CCSDS REFERENCE IMAGE SET BY DIFFERENT METHODS AT SIX BIT RATES

Evaluation indexes	Algorithm	Bit rates (bpp)					
		0.0313	0.0625	0.125	0.25	0.5	1
PSNR	SPIHT	29.26	34.36	37.51	40.10	43.34	47.14
	SPECK	34.73	36.41	38.02	40.52	43.85	47.63
	CCSDS	17.43	29.46	36.63	39.85	42.68	46.50
	JPEG2000	34.57	36.23	38.18	40.60	43.51	47.76
	BTCA	34.91	36.72	38.83	41.29	44.39	48.08
	Proposed (OADL only)	35.11	36.90	38.95	41.42	44.55	48.45
	Proposed (BTCCA only)	34.94	34.76	38.88	41.34	44.43	48.11
	Proposed	**35.17**	**36.96**	**39.02**	**41.48**	**44.58**	**48.47**
MS-SSIM	SPIHT	0.6307	0.8145	0.9024	0.9500	0.9772	0.9916
	SPECK	0.8277	0.8853	0.9320	0.9607	0.9815	0.9924
	CCSDS	0.3967	0.7886	0.8996	0.9539	0.9788	0.9917
	JPEG2000	0.8207	0.8761	0.9215	0.9568	0.9785	0.9912
	BTCA	0.8245	0.8799	0.9268	0.9591	0.9809	0.9923
	Proposed (OADL only)	0.8321	0.8845	0.9352	0.9659	0.9877	0.9956
	Proposed (BTCCA only)	0.8257	0.8821	0.9291	0.9610	0.9822	0.9928
	Proposed	**0.8339**	**0.8864**	**0.9389**	**0.9694**	**0.9892**	**0.9968**
Kappa coefficient	SPIHT	0.0231	0.0866	0.1142	0.1326	0.1601	0.2086
	SPECK	0.0928	0.1105	0.1269	0.1509	0.1652	0.2145
	CCSDS	0.0246	0.0484	0.1008	0.1343	0.1633	0.2106
	JPEG2000	0.0783	0.0837	0.0986	0.1236	0.1581	0.2181
	BTCA	0.1001	0.1137	0.1320	0.1557	0.1894	0.2290
	Proposed (OADL only)	0.1093	0.1156	0.1372	0.1585	0.1910	0.2498
	Proposed (BTCCA only)	0.1003	0.1142	0.1329	0.1563	0.1898	0.2292
	Proposed	**0.1095**	**0.1169**	**0.1387**	**0.1596**	**0.1918**	**0.2502**

TABLE VI
MS-SSIMS OF THE PROPOSED COMPRESSION METHOD AND OTHER SCAN-BASED COMPRESSION METHODS

Image	0.125bpp						0.25bpp					
	SPIHT	SPECK	CCSDS	J2K	BTCA	Proposed	SPIHT	SPECK	CCSDS	J2K	BTCA	Proposed
SanDiego1	0.8339	0.8687	0.8008	0.8506	0.8680	**0.8712**	0.9120	0.9263	0.9148	0.9222	0.9250	**0.9286**
Pentagon	0.8659	0.8911	0.8429	0.8863	0.8913	**0.8993**	0.9318	0.9428	0.9320	0.9410	0.9433	**0.9456**
NorthIsland	0.8675	0.8876	0.8504	0.8697	0.8902	**0.8917**	0.9263	0.9377	0.9276	0.9296	0.9342	**0.9388**
SanDiego2	0.8373	0.8681	0.8246	0.8457	0.8682	**0.8745**	0.9143	0.9284	0.9132	0.9196	0.9268	**0.9338**

TABLE VII
MS-SSIMS OF THE PROPOSED COMPRESSION METHOD AND OTHER SCAN-BASED COMPRESSION METHODS

Image	0.5bpp						1 bpp					
	SPIHT	SPECK	CCSDS	J2K	BTCA	Proposed	SPIHT	SPECK	CCSDS	J2K	BTCA	Proposed
SanDiego1	0.9597	0.9627	0.9627	0.9638	0.9634	**0.9666**	0.9840	0.9852	0.9848	0.9850	0.9857	**0.9868**
Pentagon	0.9687	0.9734	0.9681	0.9663	0.9718	**0.9740**	0.9877	0.9881	0.9875	0.9870	0.9887	**0.9896**
NorthIsland	0.9611	0.9631	0.9638	0.9626	0.9640	**0.9670**	0.9831	0.9841	0.9850	0.9835	0.9845	**0.9855**
SanDiego2	0.9582	0.9642	0.9595	0.9628	0.9630	**0.9659**	0.9825	0.9837	0.9835	0.9842	0.9839	**0.9851**

the same bit rate. Experimental results show the effectiveness of the proposed method.

Multi-component images, such as multi-spectral and hyperspectral images, are also very popular in remote sensing applications. Therefore, a natural idea is to apply the proposed method to the compression of multi-component images. Actually, we are now doing some research on the compression of hyperspectral images based on the proposed method. However, for the compression of hyperspectral images, an issue that needs to be considered is the bit allocation strategy among those transformed components. How to design an effective bit allocation method and combine with the proposed compression method

TABLE VIII
KAPPA COEFFICIENTS OF THE PROPOSED COMPRESSION METHOD AND OTHER SCAN-BASED COMPRESSION METHODS

Image	0.0313bpp						0.0625bpp					
	SPIHT	SPECK	CCSDS	J2K	BTCA	Proposed	SPIHT	SPECK	CCSDS	J2K	BTCA	Proposed
SanDiego1	0.75%	1.18%	0.52%	1.04%	1.18%	**1.20%**	1.27%	1.38%	1.09%	1.30%	1.38%	**1.44%**
Pentagon	0.88%	1.66%	0. 43%	1.62%	1.65%	**1.70%**	1.79%	2.50%	1.82%	2.23%	2.47%	**2.62%**
NorthIsland	1.53%	2.23%	0.79%	2.09%	2.18%	**2.29%**	2.29%	2.63%	1.97%	2.57%	2.61%	**2.77%**
SanDiego2	0.95%	1.35%	0.50%	1.33%	1.41%	**1.47%**	1.53%	1.65%	1.42%	1.72%	1.78%	**1.85%**

TABLE IX
KAPPA COEFFICIENTS OF THE PROPOSED COMPRESSION METHOD AND OTHER SCAN-BASED COMPRESSION METHODS

Image	0.125bpp						0.25bpp					
	SPIHT	SPECK	CCSDS	J2K	BTCA	Proposed	SPIHT	SPECK	CCSDS	J2K	BTCA	Proposed
SanDiego1	1.76%	1.89%	1.74%	1.84%	1.90%	**1.95%**	2.33%	2.56%	2.41%	2.48%	2.54%	**2.62**%
Pentagon	2.70%	3.14%	2.82%	3.06%	3.00%	**3.26%**	3.81%	3.93%	4.04%	4.07%	3.94%	**4.22%**
NorthIsland	2.95%	3.11%	2.98%	3.05%	3.14%	**3.28%**	3.80%	4.02%	3.89%	3.89%	3.98%	**4.12%**
SanDiego2	2.05%	2.19%	2.05%	2.12%	2.24%	**2.31%**	2.77%	2.98%	2.75%	2.76%	2.93%	**3.00%**

TABLE X
KAPPA COEFFICIENTS OF THE PROPOSED COMPRESSION METHOD AND OTHER SCAN-BASED COMPRESSION METHODS

Image	0.5bpp						1 bpp					
	SPIHT	SPECK	CCSDS	J2K	BTCA	Proposed	SPIHT	SPECK	CCSDS	J2K	BTCA	Proposed
SanDiego1	3.16%	3.25%	3.45%	3.40%	3.31%	**3.48%**	4.84%	4.78%	5.05%	4.96%	4.89%	**5.09%**
Pentagon	5.31%	5.44%	5.50%	5.34%	5.61%	**5.99%**	8.03%	8.27%	8.45%	8.35%	8.52%	**9.03%**
NorthIsland	4.98%	5.26%	5.09%	5.07%	5.30%	**5.48%**	7.45%	7.56%	7.60%	7.43%	7.72%	**8.02%**
SanDiego2	3.69%	3.81%	3.75%	3.78%	3.78%	**3.83%**	5.24%	5.30%	5.49%	5.51%	5.49%	**5.53%**

perfectly is an issue worth studying. We will research on it in the next work.

ACKNOWLEDGMENT

The authors would like to thank the handling editor and the anonymous reviewers for their careful reading and helpful remarks, which were all very valuable for improving the quality of this paper.

REFERENCES

[1] J. M. Shapiro, "Embedded image coding using zerotrees of wavelet coefficients," *IEEE Trans. Signal Process.*, vol. 41, no. 12, pp. 3445–3462, Dec. 1993.
[2] A. Said and W. A. Pearlman, "A new, fast, and efficient image codec based on set partitioning in hierarchical trees," *IEEE Trans. Circuits Syst. Video Technol.*, vol. 6, no. 3, pp. 243–250, Jun. 1996.
[3] W. A. Pearlman, A. Islam, N. Nagaraj, and A. Said, "Efficient low complexity image coding with a set-partitioning embedded block coder," *IEEE Trans. Circuits Syst. Video Technol.*, vol. 14, no. 11, pp. 1219–1235, Nov. 2004.
[4] *JPEG2000 Image Coding System*, ISO/IEC Std. 15 444-1, 2000.
[5] T. Brahimi *et al.*, "An improved wavelet-based image coder for embedded greyscale and colour image compression," *Int. J. Electron. Commun.*, vol. 73, pp. 183–192, 2017.
[6] A. Suruliandi and S. P. Raja, "Empirical evaluation of EZW and other encoding techniques in the wavelet-based image compression domain," *Int. J. Wavelets Multiresolution Inf. Process.*, vol. 13, no. 2, 2015, Art. no. 150311182946008.
[7] Z. Fang, N. Xiong, L. T. Yang, X. Sun, and Y. Yang, "Interpolation-based direction-adaptive lifting DWT and modified SPIHT for image compression in multimedia communications," *IEEE Syst. J.*, vol. 5, no. 4, pp. 584–593, Dec. 2011.
[8] Z. Wu, A. Bilgin, and W. M. Marcellin, "Joint source/channel coding for image transmission with JPEG2000 over memoryless channels," *IEEE Trans. Image Process.*, vol. 14, no. 8, pp. 1020–1032, Aug. 2005.
[9] Y. Zhang *et al.*, "Mutual information-based context template modeling for bitplane coding in remote sensing image compression," *J. Appl. Remote Sens.*, vol. 10, no. 2, 2016, Art. no. 025011.
[10] J. Yang, G. Zhu, and Q. Y. Shi, "Analyzing the effect of JPEG compression on local variance of image intensity," *IEEE Trans. Image Process.*, vol. 25, no. 6, pp. 2647–2656, Jun. 2016.
[11] Image Data Compression, CCSDS122.0-B-1, Nov. 2005. [Online]. Available: http://public.ccsds.org/publications/archive/122x0b1c3.pdf
[12] Image Data Compression, CCSDS120.1-G-1, Jun. 2007. [Online]. Available: http://public.ccsds.org/publications/archive/120x1g1e1.pdf
[13] F. García-Vílchez and J. Serra-Sagristà, "Extending the CCSDS recommendation for image data compression for remote sensing scenarios," *IEEE Trans. Geosci. Remote Sens.*, vol. 47, no. 10, pp. 3431–3445, Oct. 2009.
[14] C. Shi, J. Zhang, and Y. Zhang, "Content-based onboard compression for remote sensing images," *Neurocomputing*, vol. 191, pp. 330–340, 2016.
[15] P. Kulkarni *et al.*, "Compression of earth science data with JPEG2000," in *Hyperspectral Data Compression*. Berlin, Germany: Springer, 2006, pp. 347–378.
[16] K. K Huang and D. Q. Dai, "A new on-board image codec based on binary tree with adaptive scanning order in scan-based mode," *IEEE Trans. Geosci. Remote Sens.*, vol. 50, no. 10, pp. 3737–3750, Oct. 2012.
[17] V. B. Raju, K. J. Sankar, C. D. Naidu, and S. Bachu, "Multispectral image compression for various band images with high resolution improved DWT SPIHT," *Int. J. Signal Process. Image Process. Pattern Recognit.*, vol. 9, no. 2, pp. 271–286, 2016.
[18] X. S. Hou, M. Han, C. Gong, and X. M. Qian, "SAR complex image data compression based on quadtree and zerotree coding in discrete wavelet transform domain: A comparative study," *Neurocomputing*, vol. 148, pp. 561–568, 2015.

[19] M. V. Gashnikov and N. I. Glumov, “Onboard processing of hyperspectral data in the remote sensing systems based on hierarchical compression,” *Image Process. Syst. Inst.*, vol. 40, pp. 543–551, 2016.
[20] H. Liu *et al.*, “Quadtree coding with adaptive scanning order for space-borne image compression,” *Signal Process., Image Commun.*, vol. 55, pp. 1–9, 2017.
[21] K. K. Huang *et al.*, “Remote sensing image compression based on binary tree and optimized truncation,” *Digital Signal Process.*, vol. 64, pp. 96–106, 2017.
[22] W. Ding, F. Wu, X. Wu, S. Li, and H. Li, “Adaptive directional lifting-based wavelet transform for image coding,” *IEEE Trans. Image Process.*, vol. 16, no. 2, pp. 416–427, Feb. 2007.
[23] C. L. Chang and B. Girod, “Direction-adaptive discrete wavelet transform for image compression,” *IEEE Trans. Image Process.*, vol. 16, no. 5, pp. 1289–1302, May 2007.
[24] X. S. Hou, J. Yang, G. F. Jiang, and X. M. Qian, “Complex SAR image compression based on directional lifting wavelet transform with high clustering capability,” *IEEE Trans. Geosci. Remote Sens.*, vol. 51, no. 1, pp. 527–538, Jan. 2013.
[25] Y. Zhang, S. Negahdaripour, and Q. Li, “Low bit-rate compression of underwater imagery based on adaptive hybrid wavelets and directional filter banks[J],” *Signal Process., Image Commun.*, vol. 47, pp. 96–114, 2016.
[26] L. Zhang and B. Qiu, “Edge-preserving image compression using adaptive lifting wavelet transform,” *Int. J. Electron.*, vol. 102, no. 7, pp. 1190–1203, 2015.
[27] L. Wang, J. Bai, J. J. Wu, and G. Jeon, “Hyperspectral image compression based on lapped transform and tucker decomposition,” *Signal Process., Image Commun.*, vol. 36, no. 8, pp. 63–69, 2015.
[28] L. Zhang, L. Zhang, D. Tao, X. Huang, and B. Du, “Compression of hyperspectral remote sensing images by tensor approach,” *Neurocomputing*, vol. 147, pp. 358–363, 2015.
[29] W. Sweldens, “The lifting scheme: A construction of second generation wavelets,” *Siam J. Math. Anal.*, vol. 29, no. 2, pp. 511–546, 1998.
[30] A. R. Calderbank *et al.*, “Wavelet transforms that map integers to integers,” *Appl. Comput. Harmon. Anal.*, vol. 5, no. 3, pp. 332–369, 1998.
[31] J. A. Richards and X. Jia, *Remote Sensing Digital Image Analysis: An Introduction*, 4th ed. Berlin, Germany: Springer, 2006, pp. 10–11.
[32] J. R. Schott, *Remote Sensing: The Image Chain Approach*, 2nd ed. London, U.K.: Oxford Univ. Press, 2007, p. 209.
[33] USC-SIPI database, 2018. [Online]. Available: http://sipi.usc.edu/database/
[34] Consultative committee for space data systems, CCSDS test images, 2018. [Online]. Available: http:// cwe.ccsds.org/sls/docs/sls-dc/
[35] Y. Liu and N. K. Ngan, “Weighted adaptive lifting-based wavelet transform for image coding,” *IEEE Trans. Image Process.*, vol. 17, no. 4, pp. 500–511, Apr. 2008.
[36] B. Li, R. Yang, and H. Jiang, “Remote-Sensing image compression using two-dimensional oriented wavelet transform[J],” *IEEE Trans. Geosci. Remote Sens.*, vol. 49, no. 1, pp. 236–250, Jan. 2011.
[37] C. Shi, J. Zhang, and Y. Zhang, “A novel vision-based adaptive scanning for the compression of remote sensing images,” *IEEE Trans. Geosci. Remote Sens.*, vol. 54, no. 3, pp. 1336–1348, Mar. 2016.
[38] A. C. Shaffer, R. Juvvadi, and S. L. Heath, “Generalized comparison of quadtree and bintree storage requirements,” *Image Vision Comput.*, vol. 11, no. 7, pp. 402–412, 1993.
[39] K. K. Huang and D. Q. Dai, “A new on-board image codec based on binary tree with adaptive scanning order in scan-based mode,” *IEEE Trans. Geosci. Remote Sens.*, vol. 50, no. 10, pp. 3737–3750, Oct. 2012.
[40] C. Gaucherel, S. Alleaume, and C. Hely, “The comparison map profile method: A strategy for multiscale comparison of quantitative and qualitative images,” *IEEE Trans. Geosci. Remote Sens.*, vol. 46, no. 9, pp. 2708–2719, Sep. 2008.
[41] J. Cohen, “A coefficient of agreement for nominal scales,” *Educ. Psychol. Meas.*, vol. 20, no. 1, pp. 37–46, 1960.
[42] Z. Wang, E. P. Simoncelli, and A C. Bovik, “Multiscale structural similarity for image quality assessment,” in *Proc. IEEE Conf. Signals, Syst. Comput.*, vol. 2, 2004, pp. 1398–1402.

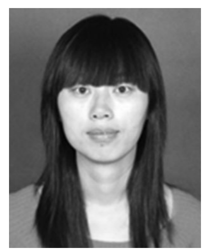

Cuiping Shi (M’13) received the M.S. degree from Yangzhou University, Yangzhou, China, in 2007, and the Ph.D. degree from the Harbin Institute of Technology, Harbin, China, in 2016.

She is currently an Associate Professor with the Department of Communication Engineering, Qiqihar University, Qiqihar, China. She is the author or co-author of more than 20 papers. Her research interests include remote sensing image compression and remote sensing image analysis and processing.

Liguo Wang (M’05) received the M.S. and Ph.D. degrees in signal and information processing from the Harbin Institute of Technology, Harbin, China, in 2002 and 2005, respectively.

From 2006 to 2008, he held a postdoctoral research position with the College of Information and Communications Engineering, Harbin Engineering University, where he is currently a Professor. He is the Author or Co-Author of two books about hyperspectral image processing and more than 130 papers in journals and conference proceedings. His research interests include remote sensing image processing and machine learning.

报告编号：**L24T2019-357**

检 索 报 告

一、检索要求

1. 委 托 人：石翠萍 Shi, CP (Shi, Cuiping)
2. 委托单位：齐齐哈尔大学
3. 检索目的：论文被 SCI-E 收录情况

二、检索范围

Science Citation Index Expanded (SCI-EXPANDED)	1975-present	网络版

三、检索结果

委托人提供的1篇论文被SCI-E收录，论文收录情况见附件一。

特此证明！

东北师范大学科技查新咨询中心

教育部科技查新工作站（L24）

（盖 章）

检索报告人：刘 丁

刘丁

2019 年 9 月 12 日

附件一： SCI-E收录情况

标题: Remote Sensing Image Compression Based on Adaptive Directional Wavelet Transform With Content-Dependent Binary Tree Codec
作者: Shi, CP (Shi, Cuiping); Wang, LG (Wang, Liguo)
来源出版物: IEEE JOURNAL OF SELECTED TOPICS IN APPLIED EARTH OBSERVATIONS AND REMOTE SENSING 卷: 12 期: 3 页: 934-949 DOI: 10.1109/JSTARS.2019.2897344
出版年: MAR 2019
Web of Science 核心合集中的 "被引频次": 0
被引频次合计: 0
使用次数 (最近 180 天): 3
使用次数 (2013 年至今): 3
引用的参考文献数: 40
入藏号: WOS:000463025100014
语言: English
文献类型: Article
作者关键词: Adaptive directional lifting (ADL); binary tree codec; compression; remote sensing images
KeyWords Plus: EFFICIENT
地址: [Shi, Cuiping] Qiqihar Univ, Dept Commun Engn, Qiqihar 161000, Peoples R China.
[Shi, Cuiping; Wang, Liguo] Harbin Engn Univ, Coll Informat & Commun Engn, Harbin 150001, Heilongjiang, Peoples R China.
通讯作者地址: Wang, LG (通讯作者)，Harbin Engn Univ, Coll Informat & Commun Engn, Harbin 150001, Heilongjiang, Peoples R China.
电子邮件地址: scp1980@126.com; wangliguo@hrbeu.edu.cn
出版商: IEEE-INST ELECTRICAL ELECTRONICS ENGINEERS INC
出版商地址: 445 HOES LANE, PISCATAWAY, NJ 08855-4141 USA
Web of Science 类别: Engineering, Electrical & Electronic; Geography, Physical; Remote Sensing; Imaging Science & Photographic Technology
研究方向: Engineering; Physical Geography; Remote Sensing; Imaging Science & Photographic Technology
IDS 号: HR3GP
ISSN: 1939-1404
eISSN: 2151-1535
29 字符的来源出版物名称缩写: IEEE J-STARS
ISO 来源出版物缩写: IEEE J. Sel. Top. Appl. Earth Observ. Remote Sens.
来源出版物页码计数: 16
输出日期: 2019-09-12

The End